



Development of selective HDAC6 inhibitors with in vitro and in vivo anti-multiple myeloma activity

Shunda Li^a, Chunlong Zhao^a, Guozhen Zhang^a, Qifu Xu^a, Qian Liu^a, Wei Zhao^a,
C. James Chou^b, Yingjie Zhang^{a,*}

^a Department of Medicinal Chemistry, Key Laboratory of Chemical Biology (Ministry of Education), School of Pharmaceutical Sciences, Cheeloo College of Medicine, Shandong University, 44 West Wenhua Road, Ji'nan, Shandong 250012, PR China

^b Department of Drug Discovery and Biomedical Sciences, South Carolina College of Pharmacy, Medical University of South Carolina, Charleston, South Carolina 29425, United States

ARTICLE INFO

Keywords:

Histone deacetylase 6
Selective inhibitor
Multiple myeloma
Anticancer
Pyrrolo[2,3-*d*]pyrimidine

ABSTRACT

Histone deacetylase 6 (HDAC6) is a promising therapeutic target for the treatment of cancers, neurodegenerative diseases and autoimmune disorders. Herein a novel series of pyrrolo[2,3-*d*]pyrimidine-based HDAC inhibitors were designed, synthesized and biologically evaluated, among which compounds **7a**, **12a1**, and **16a1** exhibited potent inhibitory activities and selectivities against HDAC6. Notably, compared with the well-known HDAC6 inhibitor Tubastatin A, our pyrrolo[2,3-*d*]pyrimidine-based HDAC6 inhibitors showed superior in vitro anti-proliferative activity against human multiple myeloma cell lines RPMI 8226, U266 and MM.1S, while maintaining the low cytotoxicity against human breast cancer cell line MDA-MB-231 and two normal cell lines. The HDAC6 selective inhibition of one representative compound **12a1** in RPMI 8226 cells was confirmed by western blot analysis. Although pyrrolo[2,3-*d*]pyrimidine is a privileged structure in many kinase inhibitors, compound **12a1** showed negligible inhibition against several kinases including JAK family members and Akt1, indicating its acceptable off-target profile. Besides, compound **12a1** exhibited desirable metabolic stability in mouse liver microsomes. The in vivo anti-multiple myeloma potency of **12a1**, alone and in combination with bortezomib, was demonstrated in a RPMI 8226 xenograft model.

1. Introduction

Zinc²⁺-dependent histone deacetylases (HDACs), a family of hydrolases involved in epigenetic regulation and post-translational modification by removing the acetyl groups from histones and non-histone proteins, have been validated to be important anticancer targets based on the successful launch of five inhibitors (vorinostat, belinostat, panobinostat, romidepsin, and chidamide) [1,2]. Amongst, panobinostat was approved in combination with bortezomib and dexamethasone for the treatment of patients with multiple myeloma who have received at least two prior treatment regimens, including bortezomib and an immunomodulatory agent [3]. However, diarrhoea and cardiac toxicities are two substantial toxicities of Panobinostat [4]. Considering that panobinostat is a pan-HDAC inhibitor with little isoform selectivity, it was presumed that isoform selective HDAC inhibitors could exhibit improved tolerability.

Among the Zinc²⁺-dependent HDACs, HDAC6 was suggested to be a

potential anti-multiple myeloma target dependent on its important roles in degradation of unfolded and misfolded ubiquitinated proteins [5]. To be specific, HDAC6 contains a zinc finger ubiquitin-binding domain and a dynein motor binding domain, through which polyubiquitinated misfolded protein cargo is recruited by HDAC6 to dynein motors for transport to aggresomes, then degraded by autophagy [6–8]. It has been demonstrated that HDAC6 inhibition could induce accumulation of polyubiquitinated proteins and inhibit the growth of multiple myelomas, especially when combined with proteasome inhibitor bortezomib [5,9]. More importantly, genetic ablation or pharmacological inhibition of HDAC6 cause no lethality or toxicity typically associated with pan-HDACs inhibition [10–13]. Currently, at least three HDAC6 inhibitors (ACY-241, ACY-1215, and CS3003) have entered clinical trials for the treatment of multiple myeloma [14]. The chemical structures and HDAC inhibitory activities of ACY-241 and ACY-1215 are present in Fig. 1.

Pyrrolo[2,3-*d*]pyrimidine is a privileged structure in drug discovery, especially in the design of protein kinase inhibitors. For example, many

* Corresponding author.

E-mail address: zhangyingjie@sdu.edu.cn (Y. Zhang).

<https://doi.org/10.1016/j.bioorg.2021.105278>

Received 17 June 2021; Received in revised form 11 August 2021; Accepted 16 August 2021

Available online 19 August 2021

0045-2068/© 2021 Elsevier Inc. All rights reserved.

JAK inhibitors including the approved drugs ruxolitinib and tofacitinib (Fig. 2) use the pyrrolo[2,3-*d*]pyrimidine group to form key hydrogen bond interactions with the hinge region of JAK proteins [17]. Besides, the clinical Akt inhibitor AZD5363 (Fig. 2) also contains the pyrrolo[2,3-*d*]pyrimidine group [18]. Interestingly, two series of pyrrolo[2,3-*d*]pyrimidine-based hydroxamates exemplified by compounds JMC-45 and BMCL-13b respectively were developed as HDAC and JAK dual inhibitors [19,20], and one series of pyrrolo[2,3-*d*]pyrimidine-based benzamides exemplified by compound EJMC-7 demonstrated potent HDAC and tubulin polymerization dual inhibition [21] (Fig. 2). These compounds indicated that pyrrolo[2,3-*d*]pyrimidine is also a privileged structure in HDAC inhibitor design. In the present research, pyrrolo[2,3-*d*]pyrimidine group was introduced to the terminal cap group of the clinical HDAC6 inhibitors (ACY-241 and ACY-1215) and the HDAC6 inhibitor pharmacophore to design a novel series of pyrrolo[2,3-*d*]pyrimidine-based hydroxamates. Structure-activity relationship (SAR) study was focused on the linker part connecting the pyrrolo[2,3-*d*]pyrimidine group and the hydroxamate group, leading to one selective HDAC6 inhibitor **12a1** with remarkable in vitro and in vivo anti-multiple myeloma potency.

2. Results and discussion

2.1. Compound design

Compounds **5a5**, **5a6**, **5b5**, **5b6** were designed by substituting pyrrolo[2,3-*d*]pyrimidine group for the terminal two phenyl groups in ACY-1215 and ACY-241. Note that the pyrimidine group in ACY-1215 and ACY-241 was replaced with phenyl group to keep the number of hydrogen bond acceptor below ten, complying with the Lipinski's rule of five (Fig. 3).

Moreover, based on the structures of reported HDAC6 inhibitors including ours [12,22–26], we can summarize a general HDAC6 inhibitor pharmacophore, where the common *N*-hydroxybenzamide group is connected with the terminal bulky aromatic cap group via one or two carbon/nitrogen atoms (Fig. 4). Introduction of the bulky aromatic pyrrolo[2,3-*d*]pyrimidine to the terminal cap of HDAC6 inhibitor pharmacophore resulted in the target compounds **7a**, **7b**, **12a1**, **12b1**, **16a0**, **16b0**, **16a1**, **16b1** (Fig. 4).

2.2. Chemistry

The procedures to synthesize all target compounds were outlined in Scheme 1. The commercially available C4-chloro-7*H*-pyrrolo[2,3-*d*]pyrimidine (**1**) reacted with various methyl aminobenzoates to afford **2a** and **2b**, which were hydrolyzed to obtain the key intermediates **3a** and **3b**. Then compound **3a** and **3b** were condensed with various methyl aminoalkanoates to produce **4a5**, **4b5**, **4a6** and **4b6**, which were

converted into hydroxamic acids **5a5**, **5b5**, **5a6** and **5b6** by NH₂OK in dry methanol, respectively. In addition, the intermediate **3a** and **3b** could react with NH₂OTHP to afford **6a** and **6b**, respectively, which were deprotected to get hydroxamic acids **7a** and **7b** under acidic condition.

N-protection of the starting material **1** with tosyl chloride led to compound **8**, which reacted with various methyl aminobenzoates to afford **9a0**, **9a1**, **9b0**, and **9b1**. The intermediates **9a1** and **9b1** could be converted into hydroxamic acids **12a1** and **12b1** according to the similar methods of synthesizing **7a** and **7b** from **2a** and **2b**. Besides, methylation of the intermediates **9a0**, **9a1**, **9b0**, and **9b1** by CH₃I led to **13a0**, **13a1**, **13b0**, and **13b1**, respectively, which could also be converted into the corresponding hydroxamic acids **16a0**, **16a1**, **16b0**, and **16b1** using the similar methods of synthesizing **7a** and **7b** from **2a** and **2b**.

2.3. In vitro HDACs inhibitory activity

Considering the clinical HDAC6 inhibitors ACY-125 and ACY-241 not only inhibit HDAC6, but also showed considerable inhibition against HDAC1, HDAC2, HDAC3 and HDAC8 (Fig. 1) [15,16], all our target compounds were firstly evaluated by determining their inhibitory rates against HDAC2, HDAC6 and HDAC8 at 0.5 μM. It has been showed that most target compounds exhibited over 50% HDAC6 inhibition at 0.5 μM, indicating their potent HDAC6 inhibitory activities (Table 1). Compounds with aliphatic linkers (**5a5**, **5a6**, **5b5**, **5b6**) also possessed considerable HDAC2 inhibitory potencies, while *N*-hydroxybenzamide-based compounds, such as **7a**, **12a1** and **16a1** showed better HDAC6 selectivity. For *N*-hydroxybenzamide-based compounds, generally, *para*-substituted *N*-hydroxybenzamides were more potent HDAC6 inhibitors than their *meta*-substituted analogs (**7a** vs. **7b**, **12a1** vs. **12b1**, **16a1** vs. **16b1**), which was in line with the HDAC6 inhibitor pharmacophore summarized in Fig. 4. The methyl group in the *N*-hydroxybenzamides showed no definitive effects on HDAC6 inhibition. To further confirm and profile their HDAC6 inhibitory activities and selectivities, the IC₅₀ values of seven selected compounds against HDAC2 and HDAC6 were determined, with the pan-HDAC inhibitor vorinostat (SAHA) and HDAC6 selective inhibitor Tubastatin A as positive controls. The results confirmed that compounds with aliphatic linkers (**5a5**, **5a6**, **5b5**, **5b6**) showed no dramatic HDAC6 selectivity over HDAC2, which was similar to SAHA. Note that compound **5a5** was even more potent against HDAC2 (IC₅₀ = 0.015 μM) than HDAC6 (IC₅₀ = 0.139 μM). Satisfyingly, *N*-hydroxybenzamide-based compounds **7a**, **12a1**, and **16a1** showed about 13-, 53- and 24-fold selectivity against HDAC6 over HDAC2, respectively. It is worth noting that the highest HDAC6-selective *N*-hydroxybenzamide **12a1** was also the most potent one, which possessed superior HDAC6 inhibitory activity (IC₅₀ = 0.010 μM) than both SAHA (IC₅₀ = 0.082 μM) and Tubastatin A (IC₅₀ = 0.085 μM).

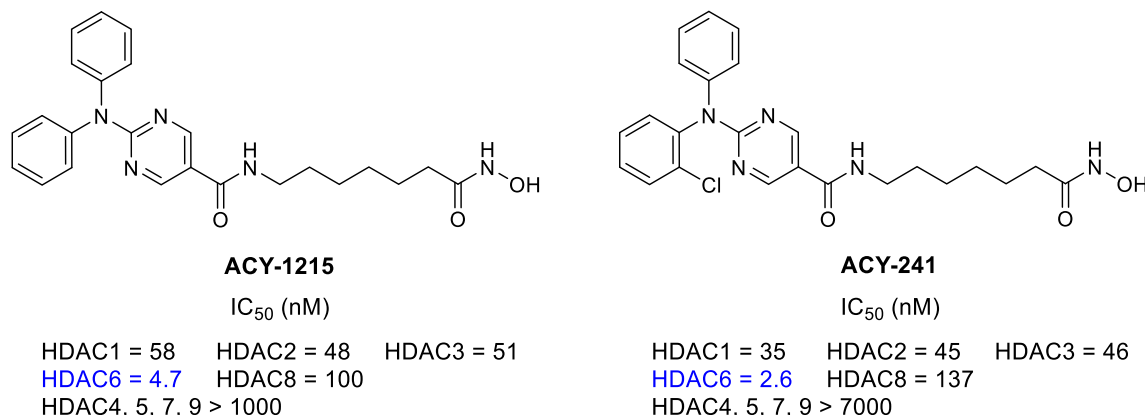


Fig. 1. The structures and HDAC inhibitory activities of two clinical HDAC6 inhibitors, ACY-1215 [15] and ACY-241 [16].

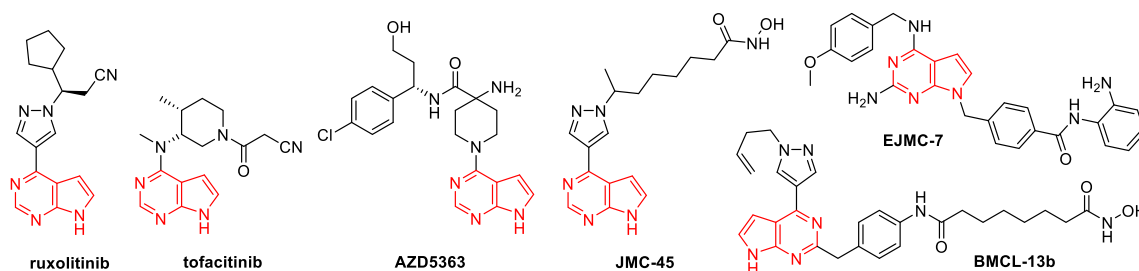


Fig. 2. The structures of representative compounds containing the pyrrolo[2,3-d]pyrimidine scaffold, which is shown in red.

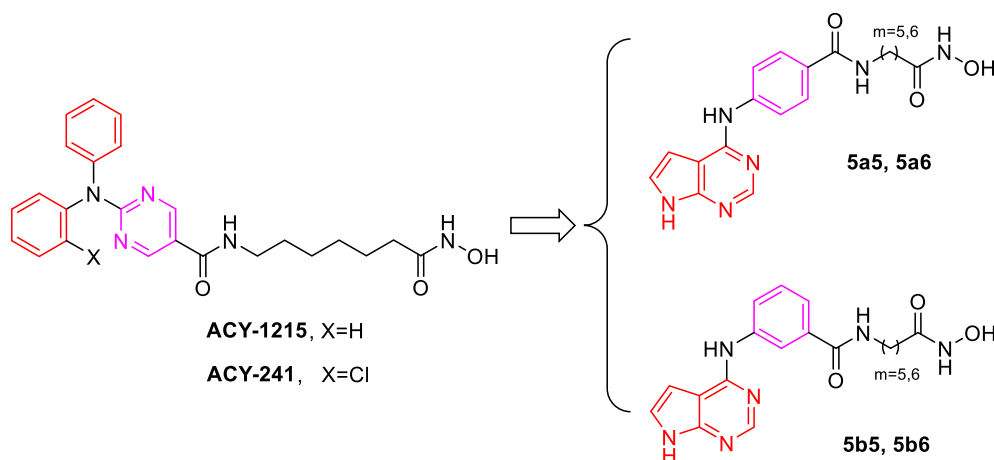


Fig. 3. The design strategy of target compounds 5a5, 5a6, 5b5, 5b6.

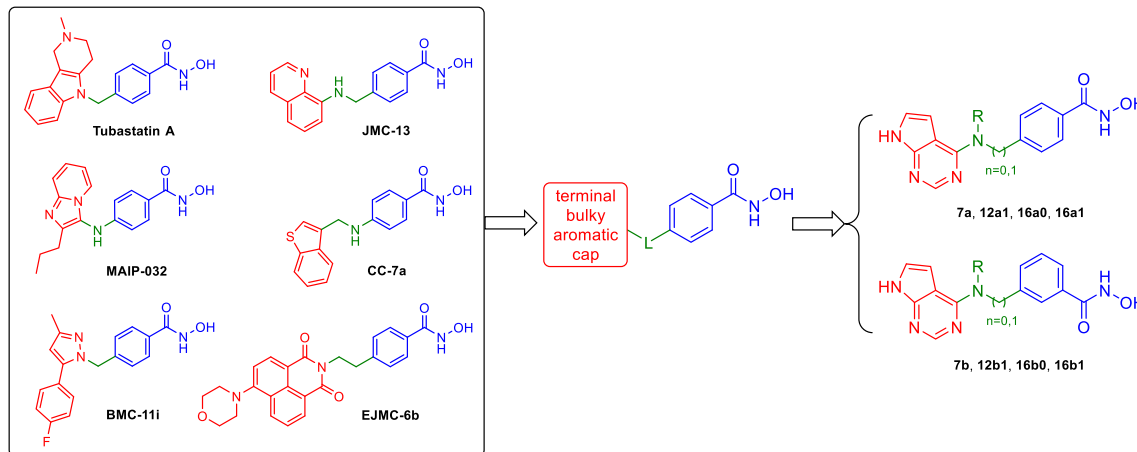
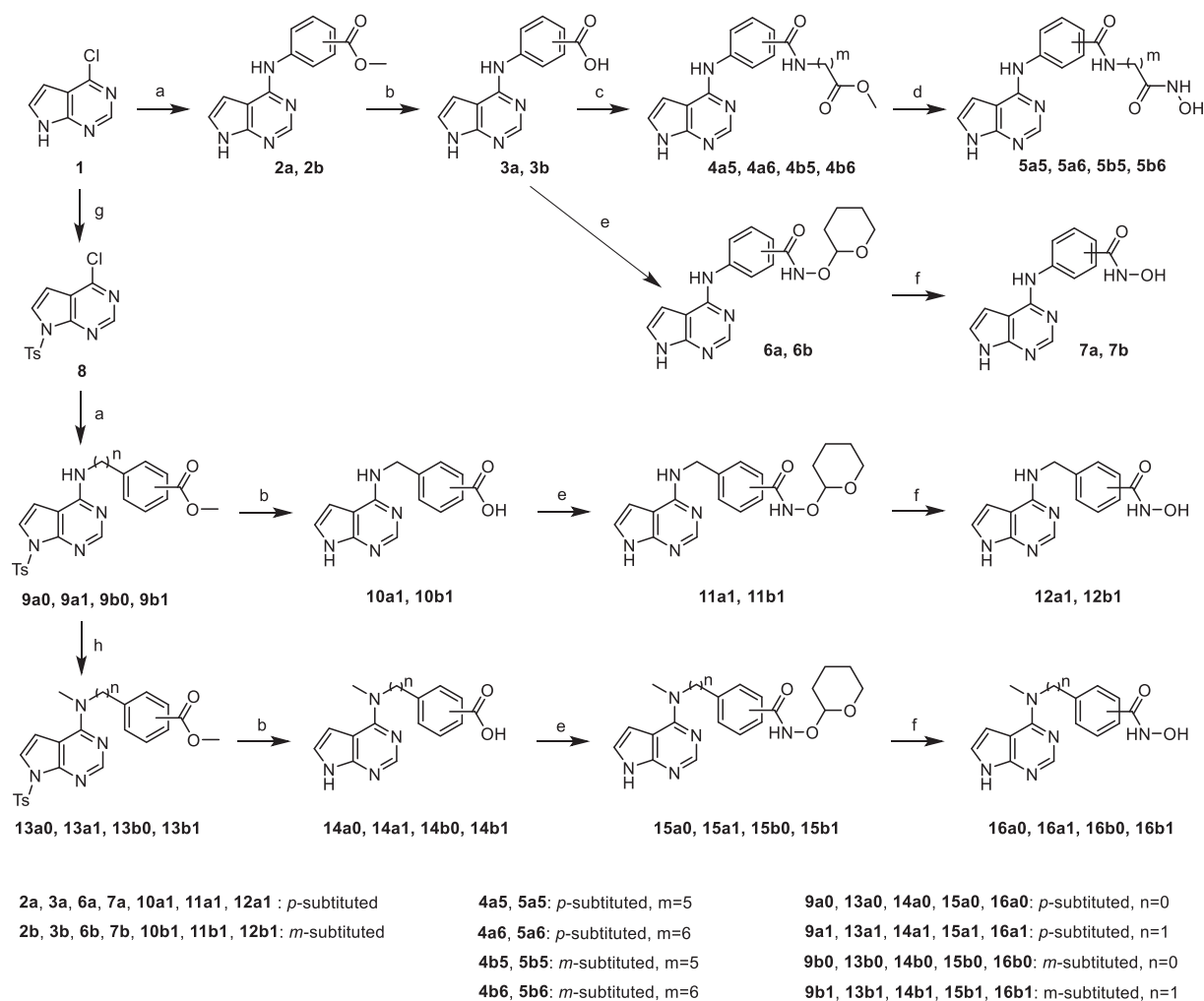


Fig. 4. The structures of reported HDAC6 inhibitors, and the design strategy of target compounds 7a, 7b, 12a1, 12b1, 16a0, 16b0, 16a1, 16b1.

2.4. In vitro anti-proliferative activity

Due to their potent HDAC6 inhibitory potencies, compounds **5b6**, **7a**, **12a1**, and **16a1** were progressed to in vitro antiproliferative assay against three human multiple myeloma cell lines (RPMI 8226, U266 and MM.1S) and one breast cancer cell line MDA-MB-231. The HDAC6 selective inhibitor Tubastatin A was used as the positive control. According to the results in Table 2, compound **5b6** exhibited greater anti-multiple myeloma potency than the other compounds, however this compound was also more cytotoxic to breast cancer cell line MDA-MB-231, which could be attributed to its more potent inhibition against HDAC2 (Table 1) and other class I HDAC isoforms. Note that compounds **7a**, **12a1**, and **16a1** could attenuate the growth of all three human

multiple myeloma cell lines more effectively than Tubastatin A, meanwhile maintained the negligible effects on MDA-MB-231, indicating the selective cytotoxicity to multiple myeloma of HDAC6 selective inhibitors. Of particular note was the HDAC6 selective inhibitor **12a1**, whose anti-multiple myeloma potency was comparable to the pan-HDAC inhibitor **5b6**. More importantly, compound **12a1** showed satisfactory safety profile in normal cells, with IC_{50} values being over 50 μ M against the human embryonic kidney cell line HEK293 and the human normal hepatic cell line LO2. Among the three tested multiple myeloma cell lines, RPMI8226 showed the most sensitivity to our inhibitors.



Scheme 1. Reagents and conditions: (a) various methyl aminobenzoate, isopropanol, conc HCl, reflux; (b) MeOH, 2.5 N NaOH, reflux; (c) various methyl aminoalkanoates, TBTU, TEA, anhydrous DMF; (d) $\text{NH}_2\text{OH}\cdot\text{HCl}$, KOH, anhydrous CH_3OH ; (e) NH_2OTHP , EDCI, HOBT, TEA, DMF; (f) HCl, anhydrous EtOAc; (g) TsCl, TEA, DMAP, DCM; (h) Cs_2CO_3 , CH_3I , DMF.

2.5. Western blot analysis

Western blot analysis was performed to evaluate the intracellular HDACs inhibitory effects of compound **12a1** in RPMI 8226 cells. The HDAC6 selective inhibitor Tubastatin A and pan-HDAC inhibitor Panobinostat were used as positive controls. From the results in Fig. 5, it was found that, similar to Tubastatin A, compound **12a1** could dose-dependently increase the intracellular levels of the HDAC6 substrate acetyl- α -tubulin without influencing the class I HDACs substrates acetyl-histone H3 and acetyl-histone H4. In contrast, the pan-HDAC inhibitor Panobinostat could increase the intracellular levels of both acetyl- α -tubulin and acetyl-histones. These results confirmed the HDAC6 inhibitory activity and selectivity of **12a1**.

2.6. In vitro kinases inhibitory activity

As discussed in the introduction part, pyrrolo[2,3-*d*]pyrimidine is widely used as hinge binding motif in many kinase inhibitors, such as the JAK inhibitors ruxolitinib, tofacitinib and the Akt inhibitor AZD5363 (Fig. 2). To preliminarily investigate the off-target effects of our pyrrolo[2,3-*d*]pyrimidine-based HDAC inhibitors, compound **12a1** was tested in kinase inhibitory assay against all four JAK family members (JAK1, JAK2, JAK3 and TYK2) and one representative Akt family member (Akt1). Our results in Table 3 revealed that the approved JAK inhibitor ruxolitinib and the clinical Akt inhibitor AZD5363 exhibited single-digit

nanomolar IC_{50} values against JAK1 and Akt1, respectively. However, at the concentration of 0.5 μM , compound **12a1** showed inhibitory rates far less than 50% against all five tested kinases, indicating a desirable off-target profile.

2.7. In vitro mouse liver microsome stability

The mouse liver microsome assay was carried out to preliminarily evaluate the metabolic stability of **12a1**. The reduced nicotinamide adenine dinucleotide phosphate (NADPH) was used as cofactor. The results in Table 4 showed that the remaining of **12a1** after 60 min incubation was 83%, indicating a good metabolic stability. In contrast, the $t_{1/2}$ of the approved hydroxamate-based HDAC inhibitor SAHA in mouse liver microsome was only 28 min [27].

2.8. In vivo antitumor activity

Based on the favorable in vitro properties of **12a1**, a RPMI 8226 xenograft model in nude mice was established to evaluate its in vivo antitumor potency with the approved proteasome inhibitor bortezomib as reference compound. Previous research demonstrated that combination of HDAC6 inhibitors and bortezomib could exhibit enhanced anti-multiple myeloma activity [5,9,24], therefore the in vivo antitumor effect of **12a1** combined with bortezomib was also evaluated. After 19 consecutive days of treatment, all treatment groups showed significant

Table 1
HDAC2, HDAC6 and HDAC8 inhibitory activities of all target compounds.

Compounds	Structures	Inhibitory rates at 0.5 μ M (IC ₅₀) ^a		
		HDAC2	HDAC6	HDAC8
5a5		99% (0.015 μ M)	89% (0.139 μ M)	23%
5a6		96% (0.095 μ M)	100% (0.022 μ M)	18%
5b5		98% (0.091 μ M)	100% (0.038 μ M)	38%
5b6		100% (0.045 μ M)	99% (0.018 μ M)	31%
7a		32% (1.24 μ M)	99% (0.090 μ M)	57%
7b		6%	45%	43%
12a1		46% (0.53 μ M)	99% (0.010 μ M)	58%
12b1		5%	64%	49%
16a0		13%	25%	57%
16a1		40% (0.70 μ M)	100% (0.029 μ M)	50%
16b0		4%	63%	59%
16b1		5%	48%	49%
SAHA		92% (0.18 μ M)	98% (0.082 μ M)	ND ^b
Tubastatin A		7% (>5 μ M)	99% (0.085 μ M)	ND ^b

^a Assays were performed in replicate ($n \geq 2$), the SD values of IC₅₀s are < 20% of the means.

^b Not determined.

tumor growth inhibition (TGI) and relative increment ratio (T/C) relative to the control group, which were presented in Table 5. The tumor growth curve was showed in Fig. 6. Remarkably, the combination treatment group presented significantly more potent tumor growth

Table 2
In vitro anti-proliferative activity of selected compounds.

Cpd	IC ₅₀ (μ M) ^a			Breast cancer MDA-MB-231	Normal cell	
	Multiple myeloma RPMI8226	U266	MM.1S		HEK293	LO2
5b6	0.46 \pm 0.12	1.60 \pm 0.31	1.74 \pm 0.27	23.3 \pm 3.8	ND ^b	ND ^b
7a	2.58 \pm 0.16	6.92 \pm 1.14	5.97 \pm 1.20	> 50	ND ^b	ND ^b
12a1	0.62 \pm 0.08	1.69 \pm 0.26	2.12 \pm 0.39	> 50	> 50	> 50
16a1	2.17 \pm 0.33	4.04 \pm 1.13	5.25 \pm 0.77	> 50	ND ^b	ND ^b
Tubastatin A	9.45 \pm 1.62	18.6 \pm 4.01	26.7 \pm 4.63	> 50	>50	> 50

^a Assay were performed in replicate ($n \geq 3$), values are shown as mean \pm SD.

^b Not determined.

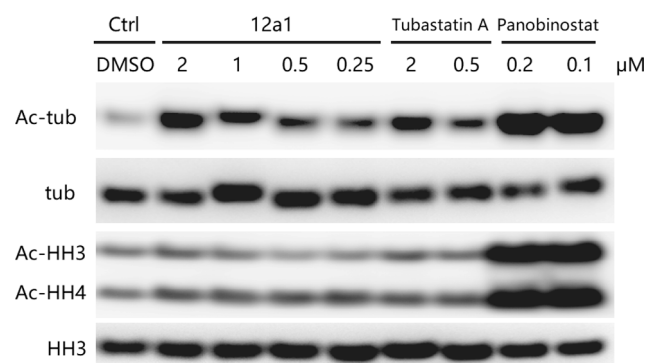


Fig. 5. RPMI 8226 cells were treated with different concentrations of compounds or DMSO for 6 h. The levels of acetyl- α -tubulin (Ac-tub), total tubulin (tub), acetyl-histone H3 (Ac-HH3), acetyl-histone H4 (Ac-HH4) and total histone H3 (HH3) were determined by immunoblotting.

Table 3
Kinases inhibitory activities of compounds 12a1, ruxolitinib and AZD5363.

	Inhibitory rates at 0.5 μ M and IC ₅₀ ^a				
	JAK1	JAK2	JAK3	TYK2	Akt1
12a1	22%	19%	37%	12%	5%
ruxolitinib	IC ₅₀ = 5.5 nM	ND ^b	ND ^b	ND ^b	ND ^b
AZD5363	ND ^b	ND ^b	ND ^b	ND ^b	IC ₅₀ = 8.4 nM

^a Assay were performed in replicate ($n \geq 2$).

^b Not determined.

Table 4
In vitro mouse liver microsome stability of compound 12a1.

	Incubation time					
	0 min	5 min	15 min	30 min	45 min	60 min
Remaining ^a	100%	95%	98%	94%	93%	83%

^a Assay were performed in replicate ($n \geq 2$).

inhibition compared with 12a1 or bortezomib alone, which could be at least partially attributed to the simultaneous inhibition of HDAC6 and proteasome. Mice body weights were monitored regularly to evaluate the toxicity of different treatment. As shown in Fig. 7, bortezomib or 12a1 treatment alone showed no obvious effects on mice body weights. Although mice treated by 12a1 and bortezomib combination lost weights slightly during treatment, they recovered gradually before the

Table 5

In vivo antitumor efficacy of **12a1**, bortezomib and their combination in a RPMI 8226 xenograft mode.

Treatment groups	T/C (%) ^a	TGI (%) ^a
12a1 (50 mg/kg/d, ip)	70	29
bortezomib (0.5 mg/kg/d, iv)	65	34
12a1 (50 mg/kg/d, ip) + bortezomib (0.5 mg/kg/d, iv)	41	61

^a Compared with the control group, all treated groups showed statistically significant ($P < 0.05$) T/C and TGI by Student's two-tailed *t* test.

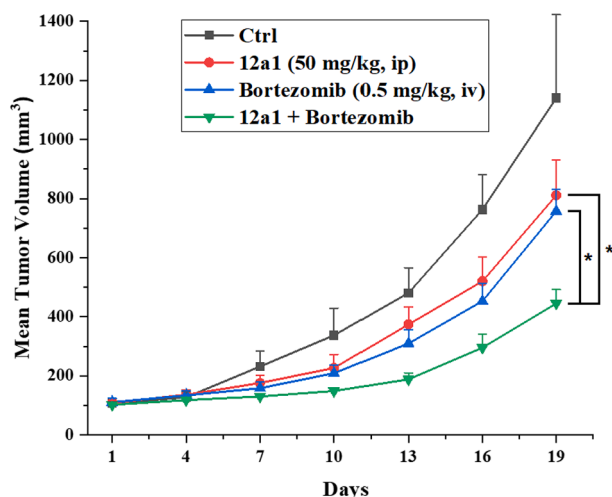


Fig. 6. Growth curve of implanted RPMI 8226 xenograft in nude mice. Data are expressed as the mean \pm SD. * $p < 0.05$ by Student's two-tailed *t* test.

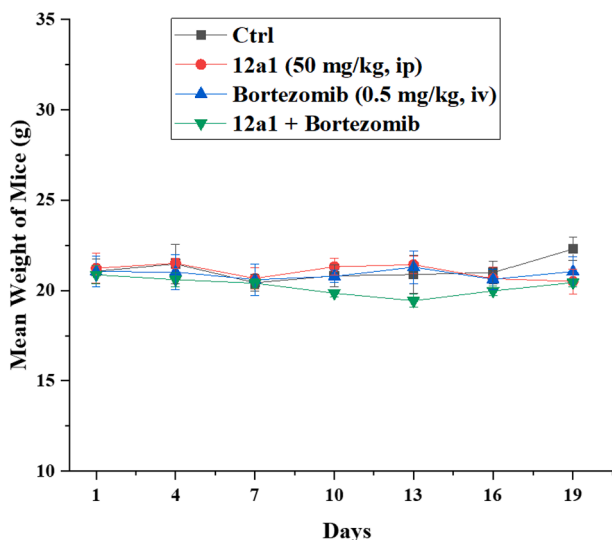


Fig. 7. Body weight curve of nude mice. Data are expressed as the mean \pm SD.

end of treatment, suggesting the acceptable toxicity of drug combination.

2.9. Molecular docking study

The proposed binding modes of **12a1** in HDAC6 and HDAC2 were investigated using Maestro 11.5 module in the Schrödinger 2018-1. As shown in Fig. 8A, compound **12a1** could fit well in the active site of HDAC6, with the hydroxamate group coordinating the catalytic Zn²⁺ bidentately and forming three hydrogen bonds with Y782, H610 and

G619, respectively. The phenyl group of **12a1** was sandwiched between F680 and F620, forming π - π stacking interactions. The pyrrolo[2,3-*d*]pyrimidine group was solvent-exposed, interacting with S568 and M682 around the entrance to the active site via two hydrogen bonds. Although **12a1** could also fit into the active site of HDAC2, with the phenyl group forming π - π stacking interaction with F155 (Fig. 8B), its hydroxamate group only displayed monodentate chelation with the catalytic Zn²⁺. Besides, only two hydrogen bonds between **12a1** and HDAC2 were observed. Therefore, the proposed bidentate hydroxamate-Zn²⁺ binding mode and more hydrogen bonds between **12a1** and HDAC6 rationalized its considerable HDAC6 inhibitory activity and selectivity.

3. Conclusion

To discover novel HDAC6 inhibitors as anti-multiple myeloma agents, a novel series pyrrolo[2,3-*d*]pyrimidine-based hydroxamates were designed, synthesized and evaluated. Structure-activity relationship (SAR) studies have been focused on the linker part between the hydroxamate group and the pyrrolo[2,3-*d*]pyrimidine group, leading to compound **12a1** with not only potent HDAC6 inhibitory activity but also considerable selectivity over HDAC2. More importantly, compound **12a1** exhibited remarkable in vitro and in vivo anti-multiple myeloma potency and no significant toxicity, which could be further developed as antitumor lead compound.

4. Experimental section

4.1. Chemistry

Unless specified otherwise, all starting materials, reagents and solvents were commercially available. ¹H NMR and ¹³C NMR spectra were obtained using a Bruker DRX spectrometer at 400 and 100 MHz respectively. Chemical shifts were reported in parts per million (ppm). Multiplicity of ¹H NMR signals was reported as singlet (s), doublet (d), triplet (t), quartet (q) and multiplet (m). ESI-MS data was recorded on an API 4000 spectrometer. High resolution mass spectra were conducted by Shandong Analysis and Test Center in Ji'nan. Melting points were determined on an electrothermal melting point apparatus and were uncorrected.

4.1.1. Methyl 4-((7H-pyrrolo[2,3-*d*]pyrimidin-4-yl)amino)benzoate (**2a**)

To a solution of **1** (0.50 g, 3.25 mmol) and methyl 4-aminobenzoate (0.54 g, 3.58 mmol) in isopropanol was added 2 drops of conc. HCl, and the mixture was heated to reflux with stirring for 10 h. The solvent was evaporated under vacuum. The crude product was purified by silica gel column chromatography (MeOH/CH₂Cl₂, 1/50 to 1/20) to afford compound **2a** (0.50 g, 57% yield), white solid. ¹H NMR (400 MHz, DMSO-*d*₆) δ 12.65 (s, 1H), 11.05 (s, 1H), 8.49 (s, 1H), 8.03 (d, $J = 8.5$ Hz, 2H), 7.95 (d, $J = 8.5$ Hz, 2H), 7.45 (t, $J = 2.8$ Hz, 1H), 7.07 (dd, $J = 3.5, 1.7$ Hz, 1H), 3.87 (s, 3H). ESI-MS, $m/z = 269.13$ [M+H]⁺.

Compound **2b** was prepared from compound **1** in a similar manner as described for compound **2a**

4.1.2. Methyl 3-((7H-pyrrolo[2,3-*d*]pyrimidin-4-yl)amino)benzoate (**2b**)

Pink solid. 71% yield. ¹H NMR (400 MHz, DMSO-*d*₆) δ 12.66 (s, 1H), 11.11 (s, 1H), 8.42 (s, 1H), 8.27 (s, 1H), 8.06 (d, $J = 7.6$ Hz, 1H), 7.83 (d, $J = 7.4$ Hz, 1H), 7.61 (t, $J = 7.7$ Hz, 1H), 7.42 (s, 1H), 6.99 (s, 1H), 3.87 (s, 3H). ESI-MS, $m/z = 269.12$ [M+H]⁺.

4.1.3. 4-((7H-pyrrolo[2,3-*d*]pyrimidin-4-yl)amino)benzoic acid (**3a**)

To a solution of the compound **2a** (0.22 g, 0.82 mmol) in MeOH (20 mL) was added 2.5 N NaOH. The mixture was heated to reflux with stirring for 2 h. Once the reaction appeared complete by TLC analysis, MeOH was evaporated from the reaction mixture, the resultant solution was cooled to 0 °C and acidified to pH 2 with 1 N HCl. The resultant precipitated product was collected by vacuum filtration and washed

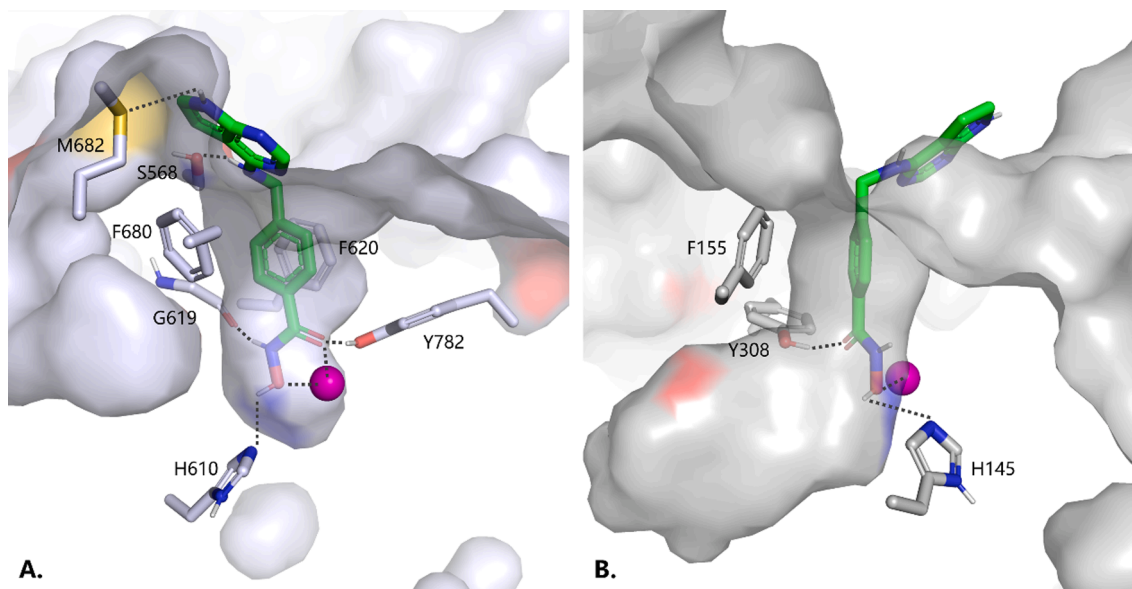


Fig. 8. The proposed binding modes of compound **12a1** (green) in the active sites of HDAC6 (**A**, bluewhite surface and sticks, PDB: 5EDU) and HDAC2 (**B**, gray surface and sticks, PDB: 3MAX). The Zn^{2+} coordination and hydrogen bonds are shown by black dashed lines.

with water to afford compound **3a** (0.16 g, 76%), white solid. 1H NMR (400 MHz, $DMSO-d_6$) δ 12.62 (s, 1H), 10.99 (s, 1H), 8.46 (s, 1H), 8.01 (d, $J = 8.4$ Hz, 2H), 7.89 (d, $J = 8.4$ Hz, 2H), 7.45 (t, $J = 2.8$ Hz, 1H), 7.07–6.98 (m, 1H). ESI-MS, $m/z = 253.06$ [M–H] $^-$.

Compounds **3b** was prepared from compound **2b** in a similar manner as described for compound **3a**.

4.1.4. 3-((7H-pyrrolo[2,3-d]pyrimidin-4-yl)amino)benzoic acid (**3b**)

White solid. 53% yield. 1H NMR (400 MHz, $DMSO-d_6$) δ 12.76 (s, 1H), 11.27 (s, 1H), 8.42 (s, 1H), 8.21 (d, $J = 2.0$ Hz, 1H), 7.97 (dd, $J = 7.9, 2.2$ Hz, 1H), 7.87 (d, $J = 7.7$ Hz, 1H), 7.62 (t, $J = 7.9$ Hz, 1H), 7.45 (t, $J = 2.9$ Hz, 1H), 6.98 (s, 1H). ESI-MS, $m/z = 253.04$ [M–H] $^-$.

4.1.5. Methyl 6-(4-((7H-pyrrolo[2,3-d]pyrimidin-4-yl)amino)benzamido)hexanoate (**4a5**)

To a solution of **3a** (0.25 g, 0.98 mmol) in anhydrous DMF (20 mL) in ice bath was added 2-(1H-benzotriazole-1-yl)-1,1,3,3-tetramethyluronium tetrafluoroborate (TBTU, 0.38 g, 1.18 mmol), followed by Et_3N (0.15 g, 1.47 mmol). 30 min later, methyl 6-aminocaproate hydrochloride (0.21 g, 1.08 mmol) and additional Et_3N (0.15 g, 1.47 mmol) were added. 6 h later, the solution was diluted by water and extracted with ethyl acetate. The combined organic extract was washed with saturated $NaHCO_3$ and brine, dried over Na_2SO_4 overnight, and the solvent was evaporated under vacuum. The crude product was purified by silica gel column chromatography ($MeOH/CH_2Cl_2$, 1/50 to 1/20) to afford compound **4a5** (0.25 g, 67% yield), yellow solid. 1H NMR (400 MHz, $DMSO-d_6$) δ 11.83 (s, 1H), 9.52 (s, 1H), 8.34 (s, 1H), 8.29 (t, $J = 5.6$ Hz, 1H), 8.00 (d, $J = 8.7$ Hz, 2H), 7.83 (d, $J = 8.7$ Hz, 2H), 7.30–7.26 (m, 1H), 6.84 (dd, $J = 3.3, 1.8$ Hz, 1H), 3.58 (s, 3H), 3.24 (q, $J = 6.7$ Hz, 2H), 2.32 (t, $J = 7.4$ Hz, 2H), 1.55 (dp, $J = 15.1, 7.3$ Hz, 4H), 1.32 (p, $J = 7.5, 6.9$ Hz, 2H).

Compounds **4a6**, **4b5** and **4b6** were prepared from compounds **3a**, **3b** in a similar manner as described for **4a5**, respectively.

4.1.6. Methyl 7-(4-((7H-pyrrolo[2,3-d]pyrimidin-4-yl)amino)benzamido)heptanoate (**4a6**)

Yellow solid. 70% yield. 1H NMR (400 MHz, Methanol- d_4) δ 11.84 (s, 1H), 9.52 (s, 1H), 8.35 (s, 1H), 8.29 (t, $J = 5.7$ Hz, 1H), 8.02 (d, $J = 8.8$ Hz, 2H), 7.84 (d, $J = 8.5$ Hz, 2H), 7.29 (t, $J = 2.8$ Hz, 1H), 6.85 (dd, $J = 3.6, 1.8$ Hz, 1H), 3.59 (s, 3H), 3.25 (q, $J = 6.7$ Hz, 2H), 2.31 (t, $J = 7.4$ Hz, 2H), 1.54 (q, $J = 7.4$ Hz, 4H), 1.32 (p, $J = 3.4$ Hz, 4H).

4.1.7. Methyl 6-(3-((7H-pyrrolo[2,3-d]pyrimidin-4-yl)amino)benzamido)hexanoate (**4b5**)

White solid. 75% yield. 1H NMR (400 MHz, Methanol- d_4) δ 11.84 (s, 1H), 9.52 (s, 1H), 8.35 (s, 1H), 8.29 (t, $J = 5.7$ Hz, 1H), 8.02 (d, $J = 8.8$ Hz, 2H), 7.84 (d, $J = 8.5$ Hz, 2H), 7.29 (t, $J = 2.8$ Hz, 1H), 6.85 (dd, $J = 3.6, 1.8$ Hz, 1H), 3.59 (s, 3H), 3.25 (q, $J = 6.7$ Hz, 2H), 2.31 (t, $J = 7.4$ Hz, 2H), 1.54 (q, $J = 7.4$ Hz, 4H), 1.32 (p, $J = 3.4$ Hz, 4H).

4.1.8. Methyl 7-(3-((7H-pyrrolo[2,3-d]pyrimidin-4-yl)amino)benzamido)heptanoate (**4b6**)

White solid. 69% yield. 1H NMR (400 MHz, $DMSO-d_6$) δ 11.78 (s, 1H), 9.47 (s, 1H), 8.41 (t, $J = 5.7$ Hz, 1H), 8.30 (s, 1H), 8.24–8.18 (m, 2H), 7.49–7.37 (m, 2H), 7.25 (t, $J = 2.8$ Hz, 1H), 6.83 (dd, $J = 3.5, 1.9$ Hz, 1H), 3.58 (s, 3H), 3.26 (q, $J = 6.7$ Hz, 2H), 2.31 (t, $J = 7.4$ Hz, 2H), 1.53 (h, $J = 7.0$ Hz, 4H), 1.35–1.28 (m, 4H).

4.1.9. 4-((7H-pyrrolo[2,3-d]pyrimidin-4-yl)amino)-N-(6-(hydroxyamino)-6-oxohexyl)benzamide (**5a5**)

KOH (28.55 g, 509 mmol) and $NH_2OH \cdot HCl$ (23.84 g, 343 mmol) were dissolved, respectively, in 70 and 120 mL of MeOH to get solution A and solution B. Then solution A was added dropwise to solution B. After filtering the precipitate (KCl), a NH_2OK solution was obtained. Compound **4a5** (0.20 g, 0.52 mmol) was dissolved in 30 mL of NH_2OK solution and stirred for 2 h. After the reaction was complete, it was evaporated under vacuum. The residue was acidified by addition of 1 N HCl to pH 5–6. The resulting precipitate was collected by filtration and dried to get the crude product, which was purified by recrystallization to get compound **5a5**, white solid (0.20 g, 83% yield). Mp: 210–212 °C. 1H NMR (400 MHz, $DMSO-d_6$) δ 11.84 (s, 1H), 10.36 (s, 1H), 9.54 (s, 1H), 8.68 (s, 1H), 8.34 (s, 1H), 8.31 (t, $J = 5.7$ Hz, 1H), 8.02 (d, $J = 8.5$ Hz, 2H), 7.84 (d, $J = 8.5$ Hz, 2H), 7.28 (t, $J = 2.5$ Hz, 1H), 6.86 (d, $J = 3.4$ Hz, 1H), 3.25 (q, $J = 6.7$ Hz, 2H), 1.97 (t, $J = 7.4$ Hz, 2H), 1.53 (dd, $J = 10.6, 5.0$ Hz, 4H), 1.30 (q, $J = 7.9$ Hz, 2H). ^{13}C NMR (101 MHz, $DMSO-d_6$) δ 169.57, 166.25, 153.63, 151.49, 151.10, 143.58, 128.24, 128.10, 123.06, 119.28, 104.54, 99.28, 32.73, 29.50, 26.63, 25.43. HRMS (AP-ESI) m/z calcd for $C_{19}H_{22}N_6O_3$ [M+H] $^+$ 383.1826, found 383.1829.

Compounds **5a6**, **5b5** and **5b6** were prepared from compounds **4a6**, **4b5** and **4b6** in a similar manner as described for **5a5**, respectively.

4.1.10. 4-((7H-pyrrolo[2,3-d]pyrimidin-4-yl)amino)-N-(7-(hydroxyamino)-7-oxohept-yl)benzamide (**5a6**)

White solid. 83% yield. Mp: 198–200 °C. ¹H NMR (400 MHz, DMSO-*d*₆) δ 11.88 (s, 1H), 10.37 (s, 1H), 9.64 (s, 1H), 8.67 (s, 1H), 8.33 (d, *J* = 8.8 Hz, 2H), 8.01 (d, *J* = 8.5 Hz, 2H), 7.84 (d, *J* = 8.5 Hz, 2H), 7.29 (t, *J* = 2.8 Hz, 1H), 6.88 (dd, *J* = 3.5, 1.7 Hz, 1H), 3.25 (q, *J* = 6.7 Hz, 2H), 1.95 (t, *J* = 7.3 Hz, 2H), 1.51 (q, *J* = 7.0 Hz, 4H), 1.29 (tq, *J* = 13.7, 7.8, 7.1 Hz, 4H). ¹³C NMR (101 MHz, DMSO-*d*₆) δ 169.62, 166.22, 153.50, 151.17, 150.68, 143.36, 128.34, 128.26, 123.13, 119.54, 104.50, 99.61, 32.72, 29.64, 28.85, 26.74, 25.59. HRMS (AP-ESI) *m/z* calcd for C₂₀H₂₄N₆O₃ [M+H]⁺ 397.1983, found 397.1987.

4.1.11. 3-((7H-pyrrolo[2,3-d]pyrimidin-4-yl)amino)-N-(6-(hydroxyamino)-6-oxohexyl)benzamide (**5b5**)

White solid. 69% yield. Mp: 208–210 °C. ¹H NMR (400 MHz, DMSO-*d*₆) δ 11.79 (s, 1H), 10.35 (s, 1H), 9.49 (s, 1H), 8.67 (s, 1H), 8.42 (t, *J* = 5.7 Hz, 1H), 8.30 (s, 1H), 8.21 (d, *J* = 8.1 Hz, 2H), 7.44 (dd, *J* = 18.5, 7.7 Hz, 2H), 7.25 (t, *J* = 2.8 Hz, 1H), 6.83 (d, *J* = 3.4 Hz, 1H), 3.26 (q, *J* = 6.7 Hz, 2H), 1.97 (t, *J* = 7.3 Hz, 2H), 1.53 (t, *J* = 7.6 Hz, 4H), 1.35–1.26 (m, 2H). ¹³C NMR (101 MHz, DMSO-*d*₆) δ 169.59, 166.81, 153.88, 151.33, 151.10, 140.95, 135.80, 128.78, 123.13, 122.82, 120.80, 119.94, 104.22, 99.31, 32.74, 29.39, 26.62, 25.42. HRMS (AP-ESI) *m/z* calcd for C₁₉H₂₂N₆O₃ [M+H]⁺ 383.1826, found 383.1834.

4.1.12. 3-((7H-pyrrolo[2,3-d]pyrimidin-4-yl)amino)-N-(7-(hydroxyamino)-7-oxohept-yl)benzamide (**5b6**)

White solid. 76% yield. Mp: 186–188 °C. ¹H NMR (400 MHz, DMSO-*d*₆) δ 12.16 (s, 1H), 10.36 (s, 1H), 10.12 (s, 1H), 8.48 (t, *J* = 5.7 Hz, 1H), 8.33 (s, 1H), 8.15 (s, 1H), 8.06 (d, *J* = 8.1 Hz, 1H), 7.60 (d, *J* = 7.7 Hz, 1H), 7.48 (t, *J* = 7.9 Hz, 1H), 7.34 (t, *J* = 2.8 Hz, 1H), 6.85 (d, *J* = 3.4 Hz, 1H), 3.26 (q, *J* = 6.7 Hz, 2H), 1.95 (t, *J* = 7.4 Hz, 2H), 1.51 (h, *J* = 7.5 Hz, 4H), 1.35–1.22 (m, 4H). ¹³C NMR (101 MHz, DMSO-*d*₆) δ 169.60, 166.50, 152.88, 149.88, 148.81, 139.52, 136.07, 129.18, 124.55, 123.67, 122.41, 121.22, 103.85, 100.35, 32.72, 29.49, 28.84, 26.72, 25.59. HRMS (AP-ESI) *m/z* calcd for C₂₀H₂₄N₆O₃ [M+H]⁺ 397.1983, found 397.1991.

4.1.13. 4-((7H-pyrrolo[2,3-d]pyrimidin-4-yl)amino)-N-((tetrahydro-2H-pyran-2-yl)oxy)benzamide (**6a**)

To a solution of **3a** (0.45 g, 1.77 mmol) in anhydrous DMF (50 mL) in ice bath, was added EDCI (0.41 g, 2.12 mmol), HOBT (0.29 g, 2.12 mmol), followed by Et₃N (0.42 g, 4.24 mmol). 30 min later, O-2-tetrahydro-2H-pyranhydroxylamine (0.25 g, 2.12 mmol) was added. 12 h later, the solution was diluted by water and extracted with ethyl acetate. The combined organic extract was washed with saturated NaHCO₃ and brine, dried over Na₂SO₄ overnight, and the solvent was evaporated under vacuum to get compound **6a** (0.12 g, 20% yield), white solid. ¹H NMR (400 MHz, DMSO-*d*₆) δ 11.85 (s, 1H), 11.51 (s, 1H), 9.57 (s, 1H), 8.35 (s, 1H), 8.03 (d, *J* = 8.6 Hz, 2H), 7.77 (d, *J* = 8.7 Hz, 2H), 7.29 (t, *J* = 2.9 Hz, 1H), 6.85 (dd, *J* = 3.5, 1.9 Hz, 1H), 5.00 (t, *J* = 3.0 Hz, 1H), 4.06–4.00 (m, 1H), 3.55–3.50 (m, 1H), 1.78–1.67 (m, 3H), 1.60–1.52 (m, 3H). ESI-MS, *m/z* = 352.15 [M–H]⁺.

Compound **6b** was prepared from compound **3b** in a similar manner as described for compound **6a**.

4.1.14. 3-((7H-pyrrolo[2,3-d]pyrimidin-4-yl)amino)-N-((tetrahydro-2H-pyran-2-yl)oxy)benzamide (**6b**)

White solid. 31% yield. ¹H NMR (400 MHz, DMSO-*d*₆) δ 11.79 (s, 1H), 11.65 (s, 1H), 9.53 (s, 1H), 8.29 (s, 1H), 8.22–8.18 (m, 2H), 7.43 (t, *J* = 7.8 Hz, 1H), 7.37 (d, *J* = 7.6 Hz, 1H), 7.25 (t, *J* = 2.9 Hz, 1H), 6.85–6.78 (m, 1H), 5.02 (t, *J* = 3.2 Hz, 1H), 4.09–4.00 (m, 2H), 1.73 (s, 3H), 1.60–1.53 (m, 3H). ESI-MS, *m/z* = 352.12 [M–H]⁺.

4.1.15. 4-((7H-pyrrolo[2,3-d]pyrimidin-4-yl)amino)-N-hydroxybenzamide (**7a**)

To a stirred solution of **6a** (0.1 g, 0.28 mmol) in 4 mL of ethyl acetate

at room temperature was added dropwise 1.0 mL of 4 N HCl in ethyl acetate. Completion of the reaction was confirmed by TLC. The resultant precipitated product was collected by vacuum filtration, affording compound **7a** (0.028 g, 37% yield), White solid. Mp: >240 °C. ¹H NMR (400 MHz, DMSO-*d*₆) δ 12.87 (s, 1H), 11.48 (s, 1H), 8.44 (s, 1H), 7.89 (d, *J* = 8.4 Hz, 2H), 7.74 (d, *J* = 8.3 Hz, 2H), 7.48 (t, *J* = 2.9 Hz, 1H), 7.05 (s, 1H). ¹³C NMR (101 MHz, DMSO-*d*₆) δ 163.87, 151.10, 144.00, 139.39, 130.57, 128.57, 125.43, 123.97, 103.67, 102.95. HRMS (AP-ESI) *m/z* calcd for C₁₃H₁₁N₅O₂ [M+H]⁺ 270.0986, found 270.0989.

Compounds **7b** was prepared from compound **6b** in a similar manner as described for compound **7a**.

4.1.16. 3-((7H-pyrrolo[2,3-d]pyrimidin-4-yl)amino)-N-hydroxybenzamide (**7b**)

Off-white solid. 62% yield. Mp: 210–212 °C. ¹H NMR (400 MHz, DMSO-*d*₆) δ 12.84 (s, 1H), 11.45 (s, 1H), 8.41 (s, 1H), 8.00 (t, *J* = 1.9 Hz, 1H), 7.81 (dd, *J* = 7.9, 2.1 Hz, 1H), 7.72 (d, *J* = 7.8 Hz, 1H), 7.58 (t, *J* = 7.8 Hz, 1H), 7.47 (t, *J* = 2.9 Hz, 1H), 6.99 (s, 1H). ¹³C NMR (101 MHz, DMSO-*d*₆) δ 163.95, 144.40, 136.94, 134.58, 130.05, 127.23, 125.27, 125.05, 123.22, 103.23, 102.52. HRMS (AP-ESI) *m/z* calcd for C₁₃H₁₁N₅O₂ [M+H]⁺ 270.0986, found 270.0987.

4.1.17. 4-Chloro-7-tosyl-7H-cyclopenta[d]pyrimidine (**8**)

To a mixture of compound **1** (1.0 g, 6.5 mmol) in 50 mL of CH₂Cl₂ were added TsCl (1.3 g, 6.9 mmol), Et₃N (1.30 g, 1.3 mmol), and DMAP (0.03 g, 0.2 mmol). The reaction mixture was stirred for 5 h at room temperature. When the reaction was complete, the solution was poured into 100 mL CH₂Cl₂, then washed with water, 1 N citric acid for 2–3 times, dried over anhydrous MgSO₄, filtered and concentrated to give compound **8** (1.81 g, 90.5% yield) as an off-white solid. ¹H NMR (400 MHz, DMSO-*d*₆) δ 8.82 (s, 1H), 8.13 (d, *J* = 4.0 Hz, 1H), 8.08–8.03 (m, 2H), 7.48 (d, *J* = 8.1 Hz, 2H), 6.97 (d, *J* = 4.0 Hz, 1H), 2.37 (s, 3H).

4.1.18. Methyl 4-((7-tosyl-7H-pyrrolo[2,3-d]pyrimidin-4-yl)amino)benzoate (**9a0**)

To a solution of **8** (0.61 g, 2.00 mmol) and methyl 4-aminobenzoate (0.34 g, 2.20 mmol) in isopropanol was added 2 drops of conc. HCl, and the mixture was heated to reflux with stirring for 2 h. Once the reaction appeared complete by TLC analysis, the reaction solution was cooled to room temperature, filtered, washed with isopropanol for 1–2 times, and dried in vacuum to afford compound **9a0** (0.76 g, 89% yield), yellow solid. ¹H NMR (400 MHz, DMSO-*d*₆) δ 9.97 (s, 1H), 8.51 (s, 1H), 8.02 (d, *J* = 8.5 Hz, 4H), 7.96 (d, *J* = 8.8 Hz, 2H), 7.78 (d, *J* = 4.0 Hz, 1H), 7.46 (d, *J* = 8.1 Hz, 2H), 7.18 (d, *J* = 4.0 Hz, 1H), 3.83 (s, 3H), 2.36 (s, 3H). ESI-MS, *m/z* = 421.13 [M–H]⁺.

Compounds **9a1**, **9b0** and **9b1** were prepared from compound **8** in a similar manner as described for compound **9a0**, respectively.

4.1.19. Methyl 3-(((7-tosyl-7H-pyrrolo[2,3-d]pyrimidin-4-yl)amino)methyl)benzoate (**9a1**)

Yellow solid. 74% yield. ¹H NMR (400 MHz, DMSO-*d*₆) δ 8.52 (t, *J* = 6.1 Hz, 1H), 8.22 (s, 1H), 8.00–7.94 (m, 2H), 7.89 (d, *J* = 8.1 Hz, 2H), 7.59 (d, *J* = 3.9 Hz, 1H), 7.42 (dd, *J* = 8.2, 4.6 Hz, 4H), 6.91 (d, *J* = 4.0 Hz, 1H), 4.75 (d, *J* = 6.0 Hz, 2H), 3.81 (s, 3H), 2.33 (s, 3H). ESI-MS, *m/z* = 437.09 [M+H]⁺.

4.1.20. Methyl 3-(((7-tosyl-7H-pyrrolo[2,3-d]pyrimidin-4-yl)amino)benzoate (**9b0**)

Yellow solid. 70% yield. ¹H NMR (400 MHz, DMSO-*d*₆) δ 10.08 (s, 1H), 8.45 (s, 1H), 8.38 (d, *J* = 1.9 Hz, 1H), 8.25–8.22 (m, 1H), 8.01 (d, *J* = 8.2 Hz, 2H), 7.75 (d, *J* = 4.0 Hz, 1H), 7.66 (dt, *J* = 7.8, 1.3 Hz, 1H), 7.51 (t, *J* = 8.0 Hz, 1H), 7.46 (d, *J* = 8.1 Hz, 2H), 7.23 (d, *J* = 4.0 Hz, 1H), 3.87 (s, 3H), 2.36 (s, 3H). ESI-MS, *m/z* = 423.12 [M+H]⁺.

4.1.21. Methyl 3-(((7-tosyl-7H-pyrrolo[2,3-d]pyrimidin-4-yl)amino)methyl)benzoate (**9b1**)

Yellow solid. 69% yield. ^1H NMR (400 MHz, DMSO- d_6) δ 8.57 (t, J = 6.0 Hz, 1H), 8.23 (s, 1H), 7.97 (d, J = 8.3 Hz, 2H), 7.92 (d, J = 1.7 Hz, 1H), 7.82 (dt, J = 7.8, 1.4 Hz, 1H), 7.63–7.57 (m, 2H), 7.47 (d, J = 7.7 Hz, 1H), 7.43 (d, J = 8.0 Hz, 2H), 6.93 (d, J = 4.0 Hz, 1H), 4.73 (d, J = 6.0 Hz, 2H), 3.82 (s, 3H), 2.35 (s, 3H). ESI-MS, m/z = 437.16 $[\text{M}+\text{H}]^+$.

Compounds **10a1**, **10b1** were prepared from **9a1**, **9b1** in a similar manner as described for compound **3a**, respectively.

4.1.22. 4-(((7H-pyrrolo[2,3-d]pyrimidin-4-yl)amino)methyl)benzoic acid (**10a1**)

White solid, 82% yield. ^1H NMR (400 MHz, DMSO- d_6) δ 11.54 (s, 1H), 8.09 (t, J = 6.7 Hz, 1H), 8.06 (s, 1H), 7.88 (d, J = 7.8 Hz, 2H), 7.44 (d, J = 7.9 Hz, 2H), 7.10 (s, 1H), 6.58 (s, 1H), 4.76 (d, J = 6.0 Hz, 2H). ESI-MS, m/z = 267.08 $[\text{M}-\text{H}]^-$.

4.1.23. 3-(((7H-pyrrolo[2,3-d]pyrimidin-4-yl)amino)methyl)benzoic acid (**10b1**)

White solid. 69% yield. ^1H NMR (400 MHz, DMSO- d_6) δ 12.94 (s, 1H), 11.60 (s, 1H), 8.14–8.09 (m, 2H), 7.93 (d, J = 1.7 Hz, 1H), 7.81 (dt, J = 7.7, 1.4 Hz, 1H), 7.63–7.57 (m, 1H), 7.45 (t, J = 7.7 Hz, 1H), 7.13–7.08 (m, 1H), 6.59 (dd, J = 3.4, 1.8 Hz, 1H), 4.77 (d, J = 6.1 Hz, 2H). ESI-MS, m/z = 267.06 $[\text{M}-\text{H}]^-$.

Compounds **11a1**, **11b1** were prepared from **10a1**, **10b1** in a similar manner as described for compound **6a**.

4.1.24. 4-(((7H-pyrrolo[2,3-d]pyrimidin-4-yl)amino)methyl)-N-((tetrahydro-2H-pyran-2-yl)oxy)benzamide (**11a1**)

Yellow solid, 37% yield. ^1H NMR (400 MHz, DMSO- d_6) δ 11.58 (s, 1H), 11.55 (s, 1H), 8.07 (s, 1H), 8.03 (t, J = 6.1 Hz, 1H), 7.71 (d, J = 8.1 Hz, 2H), 7.41 (d, J = 8.1 Hz, 2H), 7.11–7.08 (m, 1H), 6.61–6.54 (m, 1H), 4.98 (t, J = 3.1 Hz, 1H), 4.75 (d, J = 6.0 Hz, 2H), 4.08–4.00 (m, 1H), 3.53–3.48 (m, 1H), 1.73–1.68 (m, 3H), 1.57–1.50 (m, 3H). ESI-MS, m/z = 368.10 $[\text{M}+\text{H}]^+$.

4.1.25. 3-(((7H-pyrrolo[2,3-d]pyrimidin-4-yl)amino)methyl)-N-((tetrahydro-2H-pyran-2-yl)oxy)benzamide (**11b1**)

Yellow solid. 40% yield. ^1H NMR (400 MHz, DMSO- d_6) δ 11.65 (s, 1H, NH), 11.54 (s, 1H, NH), 8.08 (s, 1H), 8.01 (t, J = 6.1 Hz, 1H), 7.77 (d, J = 1.7 Hz), 7.62 (dt, J = 7.7, 1.4 Hz), 7.53–7.49 (m, 1H), 7.40 (t, J = 7.6 Hz, 1H), 7.11–7.08 (m, 1H), 6.58 (dd, J = 3.5, 1.9 Hz, 1H), 4.98 (t, J = 3.1 Hz, 1H), 4.75 (d, J = 6.0 Hz, 2H), 4.09–4.02 (m, 1H), 4.01 (d, J = 7.1 Hz, 1H), 3.51 (d, J = 11.5 Hz, 1H), 1.70 (m, 3H), 1.58–1.51 (m, 3H). ESI-MS, m/z = 366.12 $[\text{M}-\text{H}]^-$.

Compounds **12a1**, **12b1** were prepared from compounds **11a1**, **11b1** in a similar manner as described for **7a**, respectively.

4.1.26. 4-(((7H-pyrrolo[2,3-d]pyrimidin-4-yl)amino)methyl)-N-hydroxybenzamide (**12a1**)

Yellow solid. 37% yield. Mp: 222–228 °C. ^1H NMR (400 MHz, DMSO- d_6) δ 12.82 (s, 1H), 11.26 (s, 1H), 10.41 (s, 1H), 8.32 (s, 1H), 7.77 (d, J = 8.0 Hz, 2H), 7.53 (d, J = 8.0 Hz, 2H), 7.43 (t, J = 2.9 Hz, 1H), 7.12 (s, 1H), 4.96 (d, J = 6.3 Hz, 2H). ^{13}C NMR (101 MHz, DMSO- d_6) δ 164.23, 150.48, 142.81, 140.45, 132.47, 127.96, 127.62, 124.91, 102.70, 102.26, 44.88. HRMS (AP-ESI) m/z calcd for $\text{C}_{14}\text{H}_{13}\text{N}_5\text{O}_2$ $[\text{M}+\text{H}]^+$ 284.1142, found 284.1145.

4.1.27. 3-(((7H-pyrrolo[2,3-d]pyrimidin-4-yl)amino)methyl)-N-hydroxybenzamide (**12b1**)

Yellow solid. 51% yield. Mp: 156–158 °C. ^1H NMR (400 MHz, DMSO- d_6) δ 12.80 (s, 1H), 11.30 (s, 1H), 10.21 (s, 1H), 8.36 (s, 1H), 7.83 (s, 1H), 7.70 (d, J = 7.7 Hz, 1H), 7.59 (d, J = 7.7 Hz, 1H), 7.49–7.42 (m, 2H), 7.06 (s, 1H), 4.92 (d, J = 6.0 Hz, 2H). ^{13}C NMR (101 MHz, DMSO- d_6) δ 164.34, 151.27, 143.05, 137.62, 133.56, 130.77, 129.11, 126.67, 126.40, 124.83, 102.55, 102.22, 45.08. HRMS (AP-ESI) m/z

calcd for $\text{C}_{14}\text{H}_{13}\text{N}_5\text{O}_2$ $[\text{M}+\text{H}]^+$ 284.1142, found 284.1147.

4.1.28. Methyl 4-(methyl(7-tosyl-7H-pyrrolo[2,3-d]pyrimidin-4-yl)amino)benzoate (**13a0**)

To a solution of compound **9a0** (0.30 g, 0.71 mmol) in DMF (10 mL) was added cesium carbonate (0.46 g, 1.42 mmol). The reaction mixture was stirred for 30 min under nitrogen. Iodomethane (0.78 g, 5.48 mmol) was added, and the reaction mixture was stirred at room temperature for 2 h. The reaction mixture was poured into ice cold water and stirred for 30 min. The resulting precipitate was filtered, washed with water, to afford the desired compound **13a0**, yellow solid (0.23 g, 74%). ^1H NMR (400 MHz, DMSO- d_6) δ 8.46 (s, 1H), 8.08–8.03 (m, 2H), 7.96 (d, J = 8.1 Hz, 2H), 7.53–7.50 (m, 2H), 7.46–7.42 (m, 3H), 5.00 (d, J = 4.1 Hz, 1H), 3.89 (s, 3H), 3.53 (s, 3H), 2.36 (s, 3H). ESI-MS, m/z = 437.10 $[\text{M}+\text{H}]^+$.

Compounds **13a1**, **13b0** and **13b1** were prepared from compounds **12a1**, **12b0** and **12b1** in a similar manner as described for compound **13a0**, respectively.

4.1.29. Methyl 4-((methyl(7-tosyl-7H-pyrrolo[2,3-d]pyrimidin-4-yl)amino)methyl) benzoate (**13a1**)

Yellow solid. 13% yield. ^1H NMR (400 MHz, DMSO- d_6) δ 8.26 (s, 1H), 8.02–7.98 (m, 2H), 7.90 (d, J = 8.1 Hz, 2H), 7.61 (d, J = 4.2 Hz, 1H), 7.44 (d, J = 8.2 Hz, 2H), 7.35 (d, J = 8.1 Hz, 2H), 6.83 (s, 1H), 5.04 (s, 2H), 3.82 (s, 3H), 3.32 (s, 3H), 2.36 (s, 3H). ESI-MS, m/z = 451.08 $[\text{M}+\text{H}]^+$.

4.1.30. Methyl 3-(methyl(7-tosyl-7H-pyrrolo[2,3-d]pyrimidin-4-yl)amino)benzoate (**13b0**)

Yellow solid. 64% yield. ^1H NMR (400 MHz, DMSO- d_6) δ 8.43 (s, 1H), 8.05–8.03 (m, 1H), 7.95 (d, J = 8.2 Hz, 2H), 7.91 (d, J = 2.1 Hz, 1H), 7.70–7.68 (m, 2H), 7.43 (d, J = 8.1 Hz, 2H), 7.40 (d, J = 4.1 Hz, 1H), 4.81 (d, J = 4.1 Hz, 1H), 3.85 (s, 3H), 3.51 (s, 3H), 2.36 (s, 3H). ESI-MS, m/z = 437.08 $[\text{M}+\text{H}]^+$.

4.1.31. Methyl 3-((methyl(7-tosyl-7H-pyrrolo[2,3-d]pyrimidin-4-yl)amino)methyl) benzoate (**13b1**)

Off-white solid. 62% yield. ^1H NMR (400 MHz, DMSO- d_6) δ 8.28 (s, 1H), 8.00 (d, J = 8.3 Hz, 2H), 7.87–7.82 (m, 2H), 7.62 (d, J = 4.1 Hz, 1H), 7.52–7.47 (m, 2H), 7.47–7.41 (m, 2H), 6.85 (s, 1H), 5.03 (s, 2H), 3.81 (s, 3H), 3.31 (s, 3H), 2.36 (s, 3H). ESI-MS, m/z = 451.12 $[\text{M}+\text{H}]^+$.

Compounds **14a0**, **14a1**, **14b0** and **14b1** were prepared from compounds **13a0**, **13a1**, **13b0** and **13b1** in a similar manner as described for compound **3a**, respectively.

4.1.32. 4-(Methyl(7H-pyrrolo[2,3-d]pyrimidin-4-yl)amino)benzoic acid (**14a0**)

Yellow solid. 65% yield. ^1H NMR (400 MHz, DMSO- d_6) δ 11.71 (s, 1H), 8.34 (s, 1H), 8.02–7.98 (m, 2H), 7.47–7.41 (m, 2H), 6.98 (dd, J = 3.5, 2.4 Hz, 1H), 4.91 (dd, J = 3.5, 1.9 Hz, 1H), 3.58 (s, 3H). ESI-MS, m/z = 267.04 $[\text{M}-\text{H}]^-$.

4.1.33. 4-((Methyl(7H-pyrrolo[2,3-d]pyrimidin-4-yl)amino)methyl) benzoic acid (**14a1**)

Yellow solid. 66% yield. ^1H NMR (400 MHz, DMSO- d_6) δ 11.69 (s, 1H), 8.13 (s, 1H), 7.90 (d, J = 8.0 Hz, 2H), 7.35 (d, J = 8.0 Hz, 2H), 7.12 (t, J = 2.9 Hz, 1H), 6.50 (d, J = 3.5 Hz, 1H), 5.08 (s, 2H), 3.35 (s, 3H). ESI-MS, m/z = 281.08 $[\text{M}-\text{H}]^-$.

4.1.34. 3-(Methyl(7H-pyrrolo[2,3-d]pyrimidin-4-yl)amino)benzoic acid (**14b0**)

Yellow solid. 65% yield. ^1H NMR (400 MHz, DMSO- d_6) δ 13.17 (s, 1H), 11.66 (s, 1H), 8.30 (s, 1H), 7.96 (dt, J = 6.6, 1.9 Hz, 1H), 7.84 (d, J = 2.0 Hz, 1H), 7.66–7.60 (m, 2H), 6.91 (t, J = 3.0 Hz, 1H), 4.67 (dd, J = 3.6, 1.9 Hz, 1H), 3.55 (s, 3H). ESI-MS, m/z = 267.06 $[\text{M}-\text{H}]^-$.

4.1.35. 3-((Methyl(7H-pyrrolo[2,3-d]pyrimidin-4-yl)amino)methyl)benzoic acid (**14b1**)

Yellow solid. 70% yield. ^1H NMR (400 MHz, DMSO- d_6) δ 11.70 (s, 1H), 8.14 (s, 1H), 7.83 (t, $J = 3.5$ Hz, 2H), 7.51–7.42 (m, 2H), 7.13 (t, $J = 2.9$ Hz, 1H), 6.51 (d, $J = 2.7$ Hz, 1H), 5.07 (s, 2H), 3.33 (s, 3H).

Compounds **15a0**, **15a1**, **15b0** and **15b1** were prepared from compounds **14a0**, **14a1**, **14b0** and **14b1** in a similar manner as described for compound **6a**, respectively.

4.1.36. 4-(Methyl(7H-pyrrolo[2,3-d]pyrimidin-4-yl)amino)-N-((tetrahydro-2H-pyran-2-yl)ox-y)benzamide (**15a0**)

Yellow solid. 61% yield. ^1H NMR (400 MHz, DMSO- d_6) δ 11.74 (s), 11.69 (s, 1H, NH), 8.32 (s), 7.89–7.83 (m), 7.48–7.42 (m), 6.96 (dd, $J = 3.5, 2.4$ Hz, 1H), 5.03 (t, $J = 2.9$ Hz), 4.85 (dd, $J = 3.5, 1.9$ Hz), 4.15–4.02 (m), 3.56 (s, 3H), 3.55–3.51 (m, 1H), 1.74 (s, 3H), 1.62–1.51 (m, 3H). ESI-MS, $m/z = 366.15$ [M–H] $^+$.

4.1.37. 4-((Methyl(7H-pyrrolo[2,3-d]pyrimidin-4-yl)amino)methyl)-N-((tetrahydro-2H-pyran-2-yl)oxy)benzamide (**15a1**)

Yellow solid. 60% yield. ^1H NMR (400 MHz, DMSO- d_6) δ 11.68 (s, 1H), 11.59 (s, 1H), 8.13 (s, 1H), 7.71 (d, $J = 8.0$ Hz, 2H), 7.33 (d, $J = 8.0$ Hz, 2H), 7.12 (t, $J = 3.0$ Hz, 1H), 6.49 (s, 1H), 5.05 (s, 1H), 4.98 (d, $J = 3.3$ Hz, 1H), 4.06–4.00 (m, 1H), 3.53–3.48 (m, 1H), 1.71 (m, 3H), 1.56–1.51 (m, 3H). ESI-MS, $m/z = 382.06$ [M+H] $^+$.

4.1.38. 3-(Methyl(7H-pyrrolo[2,3-d]pyrimidin-4-yl)amino)-N-((tetrahydro-2H-pyran-2-yl)ox-y)benzamide (**15b0**)

Yellow solid. 60% yield. ^1H NMR (400 MHz, DMSO- d_6) δ 11.74 (s, 1H), 11.66 (s, 1H), 8.30 (s, 1H), 7.82 (dt, $J = 7.4, 1.5$ Hz, 1H), 7.77 (d, $J = 2.1$ Hz, 1H), 7.63–7.53 (m, 2H), 6.91 (t, $J = 2.9$ Hz, 1H), 4.99 (s, 1H), 4.67 (dd, $J = 3.5, 1.9$ Hz, 1H), 4.08–4.00 (m, 1H), 3.55 (s, 3H), 3.52–3.48 (m, 1H), 1.71 (brs, 3H), 1.60–1.50 (m, 3H). ESI-MS, $m/z = 368.07$ [M+H] $^+$.

4.1.39. 3-((Methyl(7H-pyrrolo[2,3-d]pyrimidin-4-yl)amino)methyl)-N-((tetrahydro-2H-pyran-2-yl)oxy)benzamide (**15b1**)

Yellow solid. 65% yield. ^1H NMR (400 MHz, DMSO- d_6) δ 11.65 (s, 1H), 11.54 (s, 1H), 8.08 (s, 1H), 8.01 (t, $J = 6.1$ Hz, 1H), 7.77 (d, $J = 1.7$ Hz, 1H), 7.62 (dt, $J = 7.7, 1.4$ Hz, 1H), 7.53–7.49 (m, 1H), 7.40 (t, $J = 7.6$ Hz, 1H), 7.11–7.08 (m, 1H), 6.58 (dd, $J = 3.5, 1.9$ Hz, 1H), 4.98 (t, $J = 3.1$ Hz, 1H), 4.75 (d, $J = 6.0$ Hz, 2H), 4.09–4.02 (m, 1H), 4.01 (d, $J = 7.1$ Hz, 1H), 3.51 (d, $J = 11.5$ Hz, 1H), 1.70 (s, 3H), 1.58–1.51 (m, 3H). ESI-MS, $m/z = 366.12$ [M–H] $^+$.

Compounds **16a0**, **16a1**, **16b0** and **16b1** were prepared from compounds **15a0**, **15a1**, **15b0** and **15b1** in a similar manner as described for compound **7a**, respectively.

4.1.40. N-hydroxy-4-(methyl(7H-pyrrolo[2,3-d]pyrimidin-4-yl)amino)benzamide (**16a0**)

White solid. 66% yield. Mp: 228–230 °C. ^1H NMR (400 MHz, DMSO- d_6) δ 12.86 (s, 1H), 11.44 (s, 1H), 8.51 (s, 1H), 7.98 (d, $J = 8.2$ Hz, 2H), 7.65 (d, $J = 8.3$ Hz, 2H), 7.21 (t, $J = 3.0$ Hz, 1H), 4.86 (s, 1H), 3.72 (s, 3H). ^{13}C NMR (101 MHz, DMSO- d_6) δ 166.93, 163.43, 145.93, 143.91, 133.63, 131.64, 129.30, 128.04, 124.63, 103.31, 102.62, 41.79. HRMS (AP-ESI) m/z calcd for $\text{C}_{14}\text{H}_{13}\text{N}_5\text{O}_2$ [M+H] $^+$ 284.1142, found 284.1147.

4.1.41. N-hydroxy-4-((methyl(7H-pyrrolo[2,3-d]pyrimidin-4-yl)amino)methyl)benza-mide (**16a1**)

White solid. 56% yield. Mp: 160–162 °C. ^1H NMR (400 MHz, DMSO- d_6) δ 12.89 (s, 1H), 11.32 (s, 1H), 8.40 (s, 1H), 7.77 (d, $J = 8.1$ Hz, 2H), 7.39 (d, $J = 7.6$ Hz, 3H), 6.72 (s, 1H), 5.21 (s, 2H), 3.49 (s, 3H). ^{13}C NMR (101 MHz, DMSO- d_6) δ 146.74, 132.29, 128.12, 127.76, 127.23, 123.26, 103.58, 102.12, 101.41, 61.84, 54.29, 28.36, 25.19, 18.76. HRMS (AP-ESI) m/z calcd for $\text{C}_{15}\text{H}_{15}\text{N}_5\text{O}_2$ [M+H] $^+$ 298.1299, found 298.1307.

4.1.42. N-hydroxy-3-(methyl(7H-pyrrolo[2,3-d]pyrimidin-4-yl)amino)benzamide (**16b0**)

White solid. 60% yield. Mp: 230–232 °C. ^1H NMR (400 MHz, DMSO- d_6) δ 12.85 (s, 1H), 11.49 (s, 1H), 8.50 (s, 1H), 8.00–7.96 (m, 2H), 7.76–7.66 (m, 2H), 7.19 (t, $J = 2.9$ Hz, 1H), 4.75 (d, $J = 3.4$ Hz, 1H), 3.73 (s, 3H). ^{13}C NMR (101 MHz, DMSO- d_6) δ 163.14, 152.45, 146.87, 143.99, 143.82, 135.18, 130.86, 130.76, 127.81, 126.86, 124.53, 103.20, 102.58, 41.78. HRMS (AP-ESI) m/z calcd for $\text{C}_{14}\text{H}_{13}\text{N}_5\text{O}_2$ [M+H] $^+$ 284.1142, found 284.1147.

4.1.43. N-hydroxy-3-((methyl(7H-pyrrolo[2,3-d]pyrimidin-4-yl)amino)methyl)benza-mide (**16b1**)

White solid. 58% yield. Mp: 134–136 °C. ^1H NMR (400 MHz, DMSO- d_6) δ 12.84 (s, 1H), 11.28 (s, 1H), 8.42 (s, 1H), 7.73–7.67 (m, 1H), 7.67 (s, 1H), 7.47 (d, $J = 6.3$ Hz, 2H), 7.41 (t, $J = 3.0$ Hz, 1H), 6.77 (s, 1H), 5.19 (s, 2H), 3.48 (s, 3H). ^{13}C NMR (101 MHz, DMSO- d_6) δ 164.16, 150.05, 143.96, 136.64, 133.74, 130.16, 129.39, 126.63, 125.57, 124.34, 104.67, 101.95, 60.78, 32.78. HRMS (AP-ESI) m/z calcd for $\text{C}_{15}\text{H}_{15}\text{N}_5\text{O}_2$ [M+H] $^+$ 298.1299, found 298.1309.

4.2. In vitro HDACs inhibition assay

HDACs inhibitory activity was determined by fluorescence assay as previously described [28]. Briefly, 10 μL of enzyme solution (HDAC2, HDAC6 or HDAC8) was mixed with different concentrations of tested compound (50 μL). The mixture was incubated at 37 °C for 5 min, followed by adding 40 μL fluorogenic substrate (Boc-Lys(acetyl)-AMC for HDAC2 HDAC6, Boc-Lys(trifluoroacetyl)-AMC for HDAC8). After incubation at 37 °C for 30 min, the mixture was quenched by addition of 100 μL of developer containing trypsin and Trichostatin A. Over another 20 min of incubation at 37 °C, fluorescence intensity was measured using a microplate reader at excitation and emission wavelengths of 390 and 460 nm, respectively. The inhibitory rates were calculated from the fluorescence intensity readout of tested wells relative to those of control wells, and the IC_{50} values were calculated using nonlinear regression with normalized dose–response fit in Prism GraphPad software.

4.3. In vitro anti-proliferation assay

All cell lines were maintained in RPMI1640 medium containing 10% FBS at 37 °C in a 5% CO_2 humidified incubator. Anti-proliferative activity was determined by the MTT (3-[4,5-dimethyl-2-thiazolyl]-2,5-diphenyl-2 h-tetrazolium bromide) method. Briefly, cells were passaged the day before dosing into a 96-well plate, allowed to grow for 12 h, and then treated with different concentrations of compound for 48 h. A 0.5% MTT solution was added to each well. After incubation for another 4 h, formazan formed from MTT was extracted by adding 200 μL of DMSO. Absorbance was then determined using an ELISA reader at 570 nm, and the IC_{50} values were calculated using nonlinear regression in Prism GraphPad software.

4.4. Western blot analysis

RPMI 8226 cells were treated with compounds or DMSO for 6 h. Then the cells were washed twice with cold PBS and lysed in ice-cold RIPA buffer. Lysates were cleared by centrifugation. Protein concentrations were determined using the BCA assay. Equal amounts of cell extracts were then resolved by SDS-PAGE, transferred to nitrocellulose membranes and probed with acetyl α -tubulin antibody, total- α -tubulin antibody, acetyl histone H3 antibody, acetyl histone H4 antibody and total histone H3 antibody, respectively. Blots were imaged using an enhanced chemiluminescence system.

4.5. In vitro kinases inhibition assay

JAK1, JAK2, JAK3, TYK2 and Akt1 inhibitory activities were tested

in HUAWEI PHARMA (Ji'nan, China) using Kinase-Glo™ Luminescent Kinase Assay, which measures kinase activity by quantitating the amount of ATP remaining in solution following a kinase reaction. In brief, the tested compounds, kinases, substrate, and ATP were diluted in kinase buffer to the indicated concentrations according to the instruction, and incubated at 30 °C for 40 min, then the Kinase-Glo reagent was added. Over an additional 15 min of incubation, the luminescence was recorded on a microplate reader (SpectraMax M5) to calculate the inhibitory rate. The IC₅₀ values were calculated using nonlinear regression with normalized dose–response fit in Prism GraphPad software.

4.6. *In vitro* mouse liver microsome stability assay

Mouse liver microsome (0.5 mg/mL) containing compound **12a1** (1.0 μM) was incubated with NADPH (1.0 mM) at 37 °C. At the specific time points, samples were added to acetonitrile to terminate the reaction, then subjected to vortex mixing for 5 min and stored in a freezer at –80 °C. Before analysis, the samples were centrifuged at 4000 rpm for 15 min. The remaining of **12a1** in the supernatants were analyzed by LC-MS/MS.

4.7. *In vivo* antitumor experiment in RPMI 8226 xenograft model

All experiments involving laboratory animals were performed with the approval of local ethics committee for animal experimentation. *In vivo* human tumor xenograft models were established according to previously described method with minor modification [24]. In brief, 1 × 10⁷ RPMI 8226 cells were inoculated subcutaneously in the right flank of male athymic nude mice (BALB/c-nu, 5–6 weeks old, Beijing HFK Bioscience Co., Ltd.). When the tumors reached an average volume of 100 mm³, the mice were randomized into four groups (n = 5) and treated with vehicle (PBS with 5% DMSO, ip), compound **12a1** (50 mg/kg/d, ip), bortezomib (0.5 mg/kg/d, iv) or **12a1** (50 mg/kg/d, ip) plus bortezomib (0.5 mg/kg/d, iv). Subcutaneous tumors were measured with a vernier caliper every three days. Tumor volumes (V) were estimated using the equation ($V = ab^2/2$, where a and b stand for the longest and shortest diameter, respectively). Mice body weights were also monitored regularly. At the end of experimental period, mice were sacrificed and dissected to weigh the tumor tissues. Tumor growth inhibition (TGI) and relative increment ratio (T/C) were calculated at the end of treatment to reveal the antitumor effects in tumor weight and tumor volume, respectively.

$TGI = (\text{the mean tumor weight of control group} - \text{the mean tumor weight of treated group}) / \text{the mean tumor weight of control group}$
 $T/C = \text{the mean RTV of treated group (T)} / \text{the mean RTV of blank control group (C)}$

RTV, namely relative tumor volume, is V_t/V_0 (V_t : the tumor volume measured at the end of treatment; V_0 : the tumor volume measured at the beginning of the treatment).

All the obtained data were used to evaluate the antitumor potency and toxicity of compounds. Data were analyzed by Student's two-tailed t test. A p-value of < 0.05 was considered statistically significant.

4.8. Molecular docking study

Compound **12a1** was docked into the active sites of HDAC6 and HDAC2 using Maestro 11.5 module in the Schrödinger 2018-1. The structures of HDAC6 (PDB: 5EDU) and HDAC2 (PDB: 3MAX) were subjected to Maestro's protein preparation module. The crystallographic protein structures were treated by adding hydrogens, removing waters, and minimizing using OPLS3 force field. The molecular structure of compound **12a1** was optimized using the LigPrep module with OPLS3 force field. The Grid file was generated using Receptor Grid Generation.

Molecular docking was carried out via Ligand Docking module with Standard-Precision (SP) mode. Other parameters were set as default values. PyMOL (<http://www.pymol.org/>) was used to visualize the docked poses and generate the figures.

Declaration of Competing Interest

The authors declare that they have no known competing financial interests or personal relationships that could have appeared to influence the work reported in this paper.

Acknowledgement

This work was supported by Natural Science Foundation of Shandong Province (Grant No. ZR2018QH007), Key Research and Development Program of Shandong Province (2017CXGC1401), Young Scholars Program of Shandong University (YSPSDU, 2016WLJH33).

Appendix A. Supplementary material

Supplementary data to this article can be found online at <https://doi.org/10.1016/j.bioorg.2021.105278>.

References

- [1] I. Ali, R.J. Conrad, E. Verdin, M. Ott, Lysine acetylation goes global: from epigenetics to metabolism and therapeutics, *Chem. Rev.* 118 (3) (2018) 340–376.
- [2] C. Zagni, G. Floresta, G. Moncino, A. Rescifina, The search for potent, small-molecule HDACs in cancer treatment: a decade after vorinostat, *Med. Res. Rev.* 37 (6) (2017) 1373–1428.
- [3] K.P. Garnock-Jones, Panobinostat: first global approval, *Drugs* 75 (6) (2015) 695–704.
- [4] http://www.accessdata.fda.gov/drugsatfda_docs/label/2015/205353s000lbl.pdf.
- [5] T. Hideshima, J.E. Bradner, J. Wong, D. Chauhan, P. Richardson, S.L. Schreiber, K. C. Anderson, Small-molecule inhibition of proteasome and aggresome function induces synergistic antitumor activity in multiple myeloma, *Proc. Natl. Acad. Sci. USA* 102 (24) (2005) 8567–8572.
- [6] D. Seigneurin-Berny, A. Verdell, S. Curtet, C. Lemerrier, J. Garin, S. Rousseaux, S. Khochbin, Identification of components of the murine histone deacetylase 6 complex: Link between acetylation and ubiquitination signaling pathways, *Mol. Cell. Biol.* 21 (23) (2001) 8035–8044.
- [7] S.S. Hook, A. Orian, S.M. Cowley, R.N. Eisenman, Histone deacetylase 6 binds polyubiquitin through its zinc finger (PAZ domain) and copurifies with deubiquitinating enzymes, *Proc. Natl. Acad. Sci. USA* 99 (21) (2002) 13425–13430.
- [8] Y. Kawaguchi, J.J. Kovacs, A. McLaurin, J.M. Vance, A. Ito, T.P. Yao, The deacetylase HDAC6 regulates aggresome formation and cell viability in response to misfolded protein stress, *Cell* 115 (6) (2003) 727–738.
- [9] T. Hideshima, J. Qi, R.M. Paranal, W.P. Tang, E. Greenberg, N. West, M.E. Colling, G. Estiu, R. Mazitschek, J.A. Perry, H. Ohguchi, F. Cottini, N. Mimura, G. Gorgun, Y.T. Tai, P.G. Richardson, R.D. Carrasco, O. Wiest, S.L. Schreiber, K.C. Anderson, J. E. Bradner, Discovery of selective small-molecule HDAC6 inhibitor for overcoming proteasome inhibitor resistance in multiple myeloma, *Proc. Natl. Acad. Sci. USA* 113 (46) (2016) 13162–13167.
- [10] Y. Zhang, S. Kwon, T. Yamaguchi, F. Cubizolles, S. Rousseaux, M. Kneissel, C. Cao, N. Li, H.L. Cheng, K. Chua, D. Lombard, A. Mizeracki, G. Matthias, F.W. Alt, S. Khochbin, P. Matthias, Mice lacking histone deacetylase 6 have hyperacetylated tubulin but are viable and develop normally, *Mol. Cell. Biol.* 28 (5) (2008) 1688–1701.
- [11] M.A. Riviello, C. Brochier, D.E. Willis, B.A. Walker, M.A. D'Annibale, K. McLaughlin, A. Siddiq, A.P. Kozikowski, S.R. Jaffrey, J.L. Twiss, R.R. Ratan, B. Langley, HDAC6 is a target for protection and regeneration following injury in the nervous system, *Proc. Natl. Acad. Sci. USA* 106 (46) (2009) 19599–19604.
- [12] K.V. Butler, J. Kalin, C. Brochier, G. Vistoli, B. Langley, A.P. Kozikowski, Rational design and simple chemistry yield a superior, neuroprotective HDAC6 inhibitor, tubastatin A, *J. Am. Chem. Soc.* 132 (31) (2010) 10842–10846.
- [13] N. Govindarajan, P. Rao, S. Burkhardt, F. Sananbenesi, O.M. Schluter, F. Bradke, J. R. Lu, A. Fischer, Reducing HDAC6 ameliorates cognitive deficits in a mouse model for Alzheimer's disease, *Embo Mol. Med.* 5 (1) (2013) 52–63.
- [14] X.H. Zhang, M. Qin, H.P. Wu, M.Y. Khamis, Y.H. Li, L.Y. Ma, H.M. Liu, A review of progress in histone deacetylase 6 inhibitors research: structural specificity and functional diversity, *J. Med. Chem.* 64 (3) (2021) 1362–1391.
- [15] L. Santo, T. Hideshima, A.L. Kung, J.C. Tseng, D. Tamang, M. Yang, M. Jarpe, J. H. van Duizer, R. Mazitschek, W.C. Ogier, D. Cirstea, S. Rodig, H. Eda, T. Scullen, M. Canavese, J. Bradner, K.C. Anderson, S.S. Jones, N. Raje, Preclinical activity, pharmacodynamic, and pharmacokinetic properties of a selective HDAC6 inhibitor, ACY-1215, in combination with bortezomib in multiple myeloma, *Blood* 119 (11) (2012) 2579–2589.

- [16] P.Y. Huang, I. Almciga-Pinto, M. Jarpe, J.H. van Duzer, R. Mazitschek, M. Yang, S. S. Jones, S.N. Quayle, Selective HDAC inhibition by ACY-241 enhances the activity of paclitaxel in solid tumor models, *Oncotarget* 8 (2) (2017) 2694–2707.
- [17] Q.W. Gao, X.W. Liang, A.S. Shaikh, J. Zang, W.F. Xu, Y.J. Zhang, JAK/STAT signal transduction: promising attractive targets for immune, inflammatory and hematopoietic diseases, *Curr. Drug Targets* 19 (5) (2018) 487–500.
- [18] M. Addie, P. Ballard, D. Buttar, C. Crafter, G. Currie, B.R. Davies, J. Debreczeni, H. Dry, P. Dudley, R. Greenwood, P.D. Johnson, J.G. Kettle, C. Lane, G. Lamont, A. Leach, R.W.A. Luke, J. Morris, D. Ogilvie, K. Page, M. Pass, S. Pearson, L. Ruston, Discovery of 4-Amino-N- (1S)-1-(4-chlorophenyl)-3-hydroxypropyl 1-(7H-pyrrolo 2,3-d p yrimidin-4-yl)piperidine-4-carboxamide (AZD5363), an Orally Bioavailable, Potent Inhibitor of Akt Kinases, *J. Med. Chem.* 56 (5) (2013) 2059–2073.
- [19] L.B. Yao, N. Mustafa, E.C. Tan, A. Poulsen, P. Singh, M.D. Duong-Thi, J.X.T. Lee, P. M. Ramanujulu, W.J. Chng, J.J.Y. Yen, S. Ohlson, B.W. Dymock, Design and synthesis of ligand efficient dual inhibitors of Janus Kinase (JAK) and histone deacetylase (HDAC) based on ruxolitinib and vorinostat, *J. Med. Chem.* 60 (20) (2017) 8336–8357.
- [20] L.B. Yao, P.M. Ramanujulu, A. Poulsen, S. Ohlson, B.W. Dymock, Merging of ruxolitinib and vorinostat leads to highly potent inhibitors of JAK2 and histone deacetylase 6 (HDAC6), *Bioorg. Med. Chem. Lett.* 28 (15) (2018) 2636–2640.
- [21] A. Singh, T.Y. Chang, N. Kaur, K.C. Hsu, Y. Yen, T.E. Lin, M.J. Lai, S.B. Lee, J. P. Liou, CAP rigidification of MS-275 and chidamide leads to enhanced antiproliferative effects mediated through HDAC1, 2 and tubulin polymerization inhibition, *Eur. J. Med. Chem.* 215 (2021), 113169.
- [22] M.K.W. Mackwitz, A. Hamacher, J.D. Osko, J. Held, A. Scholer, D.W. Christianson, M.U. Kassack, F.K. Hansen, Multicomponent synthesis and binding mode of imidazo 1,2-a pyridine-capped selective HDAC6 inhibitors, *Org. Lett.* 20 (11) (2018) 3255–3258.
- [23] J.Y. Yang, G.L. Cheng, Q.H. Xu, S.L. Luan, S.X. Wang, D. Liu, L.X. Zhao, Design, synthesis and biological evaluation of novel hydroxamic acid based histone deacetylase 6 selective inhibitors bearing phenylpyrazol scaffold as surface recognition motif, *Biorg. Med. Chem.* 26 (8) (2018) 1418–1425.
- [24] H.Y. Lee, K. Nepali, F.I. Huang, C.Y. Chang, M.J. Lai, Y.H. Li, H.L. Huang, C. R. Yang, J.P. Liou, (N-Hydroxycarbonylbenzylamino)quinolines as selective histone deacetylase 6 inhibitors suppress growth of multiple myeloma in vitro and in vivo, *J. Med. Chem.* 61 (3) (2018) 905–917.
- [25] R. De Vreese, N. Van Steen, T. Verhaeghe, T. Desmet, N. Bougarne, K. De Bosscher, V. Benoy, W. Haeck, L. Van Den Bosch, M. D’Hooghe, Synthesis of benzothiophene-based hydroxamic acids as potent and selective HDAC6 inhibitors, *Chem. Commun.* 51 (48) (2015) 9868–9871.
- [26] Y.J. Zhang, J. Yan, T.P. Yao, Discovery of a fluorescent probe with HDAC6 selective inhibition, *Eur. J. Med. Chem.* 141 (2017) 596–602.
- [27] P.R. Venkatesh, E. Goh, P.Z. Zeng, L.S. New, L. Xin, M.K. Pasha, K. Sangthongpitag, P. Yeo, E. Kantharaj, In vitro phase I cytochrome P450 metabolism, permeability and pharmacokinetics of SB639, a novel histone deacetylase inhibitor in preclinical species, *Biol. Pharm. Bull.* 30 (5) (2007) 1021–1024.
- [28] X.W. Liang, J. Zang, X.Y. Li, S. Tang, M. Huang, M.Y. Geng, C.J. Chou, C.P. Li, Y. C. Cao, W.F. Xu, H. Liu, Y.J. Zhang, Discovery of Novel Janus Kinase (JAK) and Histone Deacetylase (HDAC) dual inhibitors for the treatment of hematological malignancies, *J. Med. Chem.* 62 (8) (2019) 3898–3923.